Influence of defect density on the gas sensing properties of multi-layered graphene grown by chemical vapor deposition

Ricciardella, Filiberto; Vollebregt, Sten; Tilmann, Rita ; Hartwig, Oliver ; Bartlam, Cian ; Sarro, Pasqualina M.; Sachdev, Hermann ; Duesberg, Georg S.

Important note
To cite this publication, please use the final published version (if applicable).
Please check the document version above.

Influence of defect density on the gas sensing properties of multi-layered graphene grown by chemical vapor deposition

Filiberto Ricciardella [a,b,1,*], Sten Vollebregt [a], Rita Tilmann [b], Oliver Hartwig [b], Cian Bartlam [b], Pasqualina M. Sarro [a], Hermann Sachdev [b], Georg S. Duesberg [b]

[a] Department of Microelectronics, Delft University of Technology, Feldmannweg 17, 2628 CT Delft, the Netherlands
[b] Institute of Physics, Universitaet der Bundeswehr Muenchen, Werner-Heisenberg-Weg 39, 85577 Neubiberg, Germany

A B S T R A C T

Chemical vapor deposition (CVD) has been demonstrated as a highly promising technique for the production of graphene on large scale and enabling tunability of the intrinsic defects of the films during the synthesis.

In this work, we report on the correlation between the density of defects (DoD) and the kinetics of interaction of multi-layered graphene (MLG) with nitrogen dioxide (NO_2) used as a target gas. We grow MLG on a pre-patterned molybdenum (Mo) catalyst layer, tailoring the DoD while growing MLG at temperatures from 850 °C to 980 °C. Analysing the Raman spectra, we show the lowering of the DoD as well as a quality dependence of MLG as a function of the growth temperature. The chemi-resistors based on MLG grown at different temperatures unambiguously highlight that, both during the exposure and the subsequent purge phase, the more defective the MLG, the more intense the NO_2's molecules interaction with MLG. Our results significantly mark a step forward in tuning the sensing properties of MLG without the need of any post-processing of the material after synthesis.

1. Introduction

The deviation from the perfect lattice structure of graphene and the presence of defects do not necessarily represent a downside. Conversely, the imperfections make possible to tailor the local properties, achieving new functionalities [1–6]. Especially in the field of sensing, both theoretical and experimental studies have widely shown that introducing defects, such as vacancies, interstitial atoms, dislocations or dopants, increases the sensitivity towards the analytes compared to the pristine material [7–19]. In fact, defects are often centers of chemical activity [20].

The most explored line of research is typically oriented to intentionally induce defects or damages into the lattice of the graphene after the synthesis in order to enhance the sensitivity towards the gasses [14,21,22]. A less costly and more efficient solution could focus on harnessing the defects intrinsically ascribed to the morphology of the sensing material. In a prior work we have addressed the effects of a particular kind of defects, *i.e.* edge defects, on the sensing properties of multi-layered graphene (MLG) [23]. However, it is well known that high-quality graphene grown on large-scale by chemical vapor deposition (CVD) [24–26] can also spontaneously acquire defects during the nucleation and growth period [14,20,27–32]. While the formation of defects is independent from the used catalytic metal substrate, the density of defects (DoD) in CVD-grown graphene can be affected by the catalyst [33].

In this paper, we experimentally investigate the correlation between the DoD and the kinetics of interaction with a target gas. We tuned the level of defects during the growth process of the material through the CVD technique by growing MLG at different temperatures (850 °C, 890 °C, 935 °C, 980 °C). No post-growth process was performed. The analysis hereby presented focuses on the properties of the active medium rather than on the study of sensors' features. In this view, we adopted NO_2 as a target gas since, in prior works, a high affinity between CVD-grown MLG and NO_2 has been shown compared to other analytes [10,34–36]. In addition, reporting in this manuscript the same investigation performed upon other target gasses can mislead the readers. To obtain more in-

---

sight into the sensing properties of MLG towards NO_2, we used the simplest transduction structure, *i.e.* a resistor, acting as a chemiresistor when exposed to the target gas. Furthermore, we used ambient conditions as our aim is to investigate the sensing properties of the active layers in an atmosphere similar to the real operating environment of gas sensors. However, despite of working in humid environment, the interference of water is rather negligible, due to the low reactivity of MLG upon humidity, as detailed in previous work [37] where it is shown that the contribution of relative humidity is three orders of magnitude lower compared to the signal induced by the analyte itself.

2. Material and methods

MLG was grown by CVD on pre-patterned Mo catalyst in an AIXTRON BlackMagic Pro in Ar/H_2 atmosphere, as further detailed in prior reports [34,35,38–41]. Four different values of growth temperature were used: 850 °C, 890 °C, 935 °C or 980 °C. The time that the catalyst was exposed to CH_4 was kept at 20 min (Figure S1) except that for the growth at 980 °C, when growth time was set at 5 min.

The grown material was investigated through a Renishaw inVia Reflex spectrometer equipped with a 633 nm He–Ne laser. The output power of the laser was 2.3 mW using a 50 × objective with a numerical aperture of 0.50. To determine the morphology of MLG, a Bruker nanoIR2 AFM-IR instrument was used with a PR-EX-T125 cantilever operating in tapping mode at a rate of 0.3 Hz.

X-ray Photoelectron Spectroscopy (XPS) was performed to examine the elemental composition of MLG film. The XPS measurements were carried out using a PHI VersaProbe III instrument equipped with a micro-focused monochromated Al Kα source (1486.6 eV) and dual beam charge neutralization. Core level spectra were recorded with PHI SmartSoft-VP software using an x-ray beam with approximately 200 μm spot size and were processed with PHI MultiPak 9.8. The sputter depth profiles were conducted using 0.5 keV Ar+ ions.

Resistors based on CVD-grown MLG were fabricated adopting the transfer-free process [41].

The growth of MLG occurred on top of Mo layer which was prepatterned by lithographic steps and dry etching before the MLG growth. The catalyst layer beneath MLG was subsequently removed by wet etching, immersing for 1–2 min the 4″-wafer into H_2O_2 solution concentrated at 31% (vol.)(D-Basf). Afterwards, MLG dropped on the SiO_2/Si substrate on the pre-defined locations, thus circumventing any transfer step of MLG to a different target substrate. After the Cr/Au (10/100 nm) electrodes deposition using a lift-off process, the current-voltage (I–V) measurements were performed through a semiautomatic probe-station equipped with an Agilent 4156C semiconductor parameter analyser. The devices were then bonded using Al wires (30 μm diameter) to carry out the sensing measurements.

The detection experiments were carried out in a customized gas sensor characterization system (GSCS) setting temperature, pressure and relative humidity (RH) at (22 ± 2) °C, (1.00 ± 0.05) bar and 50%, respectively. The total flow of target (NO_2) and buffer gas (N_2) injected in the chamber was kept at 500 sccm. The GSCS, a stainless steel chamber (40 cl), was placed in a thermostatic box and provided with an electrical grounded connector for bias and conductance measurements. The different gas concentrations were obtained by programmable mass flow controllers (MFCs). During the measurements, the sensors were biased at 1 V in DC voltage with a Precision Power Supply (TTi QL355T) and the current values were recorded by a high resolution picoammeter (Keithley 6485).

The sensors were exposed to twelve sequential pulses at different NO_2 concentrations ranging from 1.5 down to 0.12 ppm. The baseline preceding the first exposure lasts 30 min to enable the
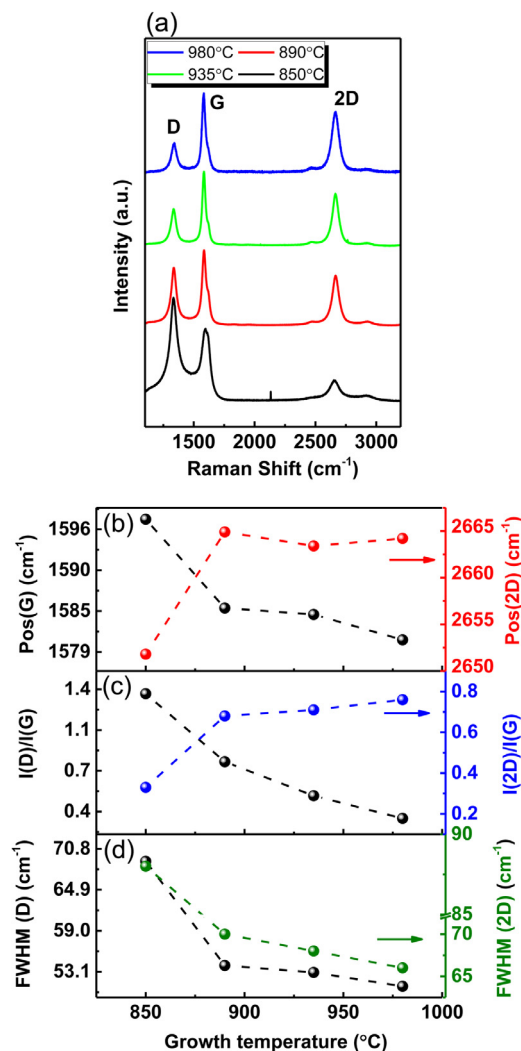
Fig. 1. (a) Representative Raman spectra of MLG grown at different temperatures. Each profile, normalized to the intensity of the G band, is averaged from 3 spots acquired along the sample. (b) Position of G- (black spots) and 2D-band (red spots). (c) Intensity ratio between D and G band (black dots) or between 2D and G band (blue dots). (d) FWHM (D) (black dots) and FWHM (2D) (green dots). The values in the stack are plotted as a function of the growth temperature of MLG.

stabilization of the sensors in the test chamber. Each step lasted 4 min, preceded and followed by baseline and purge phases, lasting 20 min each, under a N_2 atmosphere.

3. Results and discussion

Fig. 1a displays four representative Raman spectra of the materials grown at different temperatures. The profiles exhibit the most prominent features of the graphitic materials, named as D, G and 2D band. The D-band originates from the disorder present in the crystal and involves the contributions of each kind of defect, defect being defined as anything which breaks the symmetry of the crystal [42]. The G-band is related to the C−C bond while the 2D-band, the second-order of the D-band, is generally associated to graphite-like materials [43]. The spectra display some differences related to parameters such as position (Pos), intensity (I) and fullwidth at half maximum (FWHM) of the three bands (Fig. 1b-c-d).

The position of the bands G (~1590 cm^{-1}) and 2D (~2660 cm^{-1}) (Fig. 1b) are significantly different between the material grown at 850 °C (later referred as MLG850) and the other three deposition temperatures. At the lowest temperature, Pos(G) (Pos(2D))

Table 1
Parameters of the Raman spectra extracted from Fig. 1.

Growth temperature [°C]	I(D)/I(G)	I(2D)/I(G)	FWHM (D) [cm^{-1}]	FWHM (2D) [cm^{-1}]	Pos (D) [cm^{-1}]	Pos (G) [cm^{-1}]	Pos (2D) [cm^{-1}]
850	1.4	0.33	69	88	1336	1597	2652
890	0.8	0.68	54	70	1337	1585	2665
935	0.5	0.71	53	68	1335	1584	2663
980	0.3	0.76	51	66	1337	1581	2664

shows the maximum (minimum) followed by a drastic downshift (upshift) and subsequent unchanged position while increasing the growth temperature. It is worth to note that the position of the three bands are consistent with the results reported elsewhere using a red laser as an excitation wavelength, provided that the 2D Raman mode is dispersive with the energy of the incident laser [44–47]. Since the position of the bands are related to the properties of the material [44–47], the variation of the parameters between MLG850 and the other MLGs provides a first indication of the morphological differences among such materials. The last observation is strengthened by analysing the other metrics extracted from the Raman spectra. For instance, I(D)/I(G), *i.e.* the ratio between the intensities of D and G bands (black dots in Fig. 1c), presents the highest value at 850 °C, progressively reduced as the growth temperature increases. This outcome is of particular relevance as it proves the lowering of the defects' density by increasing the growth temperature while adopting Mo as a metal catalyst. The trend is in close agreement with the results shown by the Eres' group [48] despite of the slight different growth process by CVD on copper or Mo catalyst [49–52].

Finally, the metric based on I(2D)/I(G) even shows a remarkable difference between MLG850 and the other three MLG (blue dots in Fig. 1c). While I(2D)$_{MLG850}$/I(2D)$_{MLG890}$ ~ 0.5 when normalized to the G peak intensity, the largest variation among the other three samples grown at different temperatures is 0.12, indicating unchanged values within error. As such, I(2D)/I(G) rising from 0.3 to 0.8 shows that the higher growth temperature results in the transformation from a material more similar to graphite to multi-layers of graphene [2,37,38,43,53–55]. The transformation of MLG as a function of the growth temperature is further displayed by the progressive decrease of both FWHM(D) and FWHM(2D) (Fig. 2d). Focusing on the 2D-band, it should be noticed that the band is distinctly sharp and does not present any shoulder at lower wavenumbers, as generally observed in graphite spectrum. The last feature of the 2D-band suggests the structure of MLG being grown as a turbostratic material, independent from the temperature used [37,43,56].

Table 1 reports the overview of the values obtained from Fig. 1, including Pos(D) that was not plotted previously as the negligible shifts around 1340 cm^{-1} do not provide relevant insights on the transformation of MLG.

The Raman analysis enables to draw the first conclusions about the grown materials. At 850 °C, MLG results to be highly defective with a partly degraded structure of the lattice, as depicted by the low intensity of the 2D-band [55]. As the growth temperature increases, the DoD is smoothly lowered as well as a more organized structure is induced.

The nature of the as grown multi-layered structures is assessed in more detail by the AFM investigation. The corresponding topography is reported in Fig. 2a-d for each of the four samples.

Fig. 2a-b displays a relatively smooth material, compared to Fig. 2c-d. The thickness of about 10 nm can be determined from the inset of Fig. 2a while the roughness (R$_a$) is about 1 nm, as being determined from the close up (Figure S3). The morphology of the other three MLG samples (Fig. 2c-d), and especially the value of the roughness of MLG980 (Table 2), indicates that some residues might be trapped underneath MLG980 as resulting
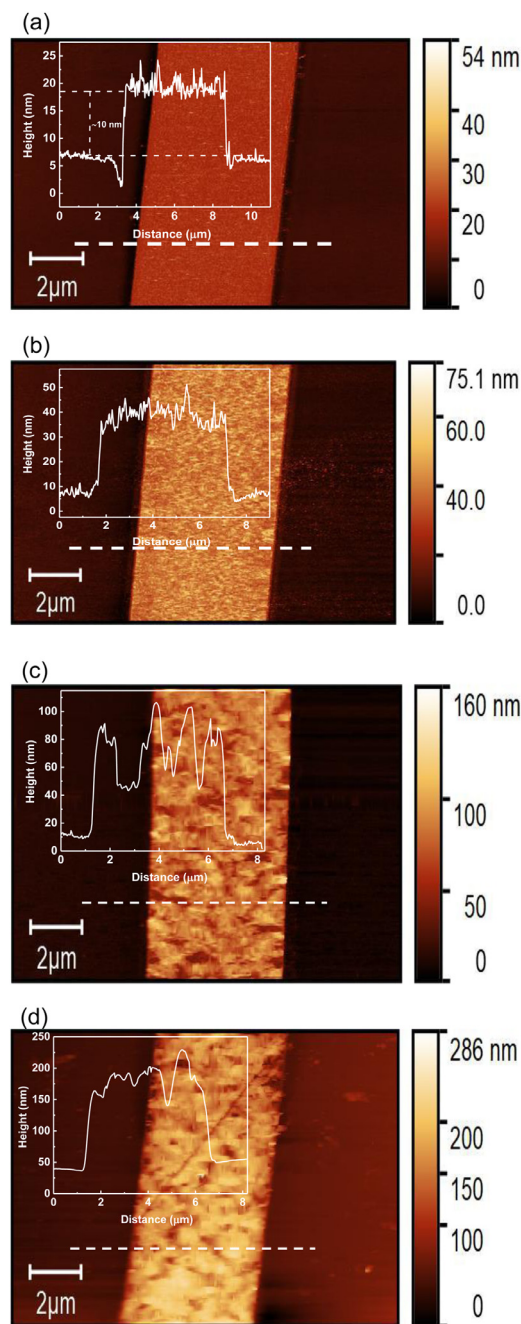
Fig. 2. AFM image of MLG grown at (a) 850 °C, (b) 890 °C, (c) 935 °C and (d) 980 °C. The insets reports the step-height profiles determined along the dashed lines drawn in each panel. The dip in the profile of panel (a) is probably a hollow in the SiO$_2$ film and might be ascribed to the limited selectivity of the plasma etching used when patterning the Mo layer [37] (Figure S2).

Table 2
Roughness of the samples grown at different temperatures.

Growth temperature (°C)	Roughness (nm)
850	1
890	4
935	15
980	28
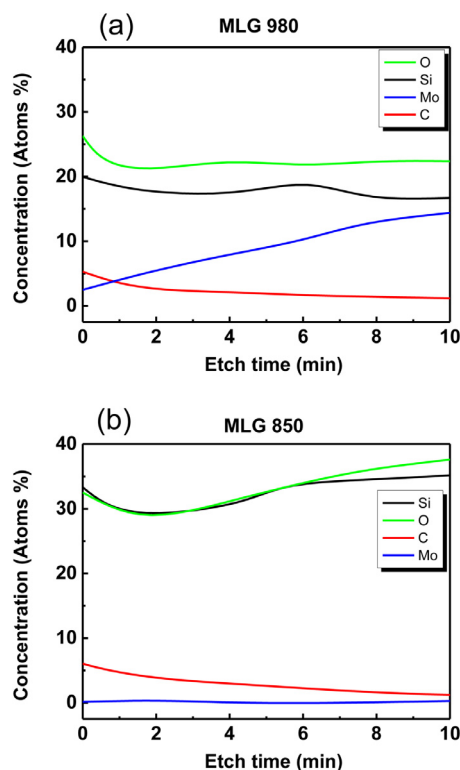
Fig. 3. XPS depth profiles acquired from (a) MLG980 and (b) MLG850.

Fig. 4. I–V curves recorded on the resistors based on MLG. Inset: optical image of one device with the MLG-bar enclosed in the dashed rectangle. The sensing area is about 1030 μm^2.

from the transfer-free process or there might be induced stress caused by the graphitization. Due to the different levels of observed roughness, we mainly based our outcomes on the Raman investigation, which enables to explore deeper the intrinsic features of the material beyond the surface.

The XPS profile acquired on MLG980 (Fig. 3a) confirmed that, while increasing the milling by Ar ion, some residues of the sacrificial Mo layer (blue line) were found. It is likely that those residues either remained accidentally nestled underneath the carbonaceous layer or diffused into SiO_2 during the growth temperature of MLG at 980 °C, affecting the roughness of the sample. Conversely, the elemental profile of MLG850 (Fig. 3b) shows concentration of Mo atoms lower than the instrument resolution (<0.1 atomic%).

The rough morphology of MLG980 made it difficult to exactly extract the thickness, nevertheless in our prior works [37,54,57] using analogous growth recipes, we obtained MLG with thickness of about 10 nm, in close agreement with the result of MLG850.

To gain more insights into the influence of DoD on the sensing properties, we fabricated four devices based on MLG. Fig. 4 shows the I–V characteristics of the devices (inset).

The linearity of the curves testifies that the devices behave as resistors and it further highlights the difference between MLG850 and the MLGs grown at the other three temperatures. The resistor based on MLG850 shows sheet resistance (R_s) significantly higher (~7 kΩ/sq) than the other three values, which are all in the range of 1 kΩ/sq. Such a large difference might be ascribed to the com-

plete absence of a well-defined structure at the nanoscale in the material grown at 850 °C compared to the others, which have a more defined structure, resulting in a lower conductivity. This argument is supported by the Raman measurements previous discussed.

The resistors were subsequently exposed to NO_2 and the transient behavior is reported in Fig. 5a.

Independently from the growth temperature of MLG, each sensor shows a similar behavior. During each pulse of the analyte, the current continuously rises and does not reach a steady state. When the analyte flow is stopped, the current starts to decrease. The magnification of the two steps, exposure and purge phase, reveals remarkable differences between MLGs grown at different temperatures (Fig. 5b). It is well known that different adsorption mechanisms between the sensing layer and the gas molecules result in different slopes in the dynamic current behavior [39,58]. We therefore suggest that analyzing the slope of the signal during the single NO_2 exposure periods or the constant time of the purge phase provides more insight on the influence of DoD on the sensing properties.

As an example, Fig. 5c displays the fit of the current recorded during the pulse at 1.5 ppm of NO_2 (see right y-axis of Fig. 5b) (Figure S4). Fig. 5d report the current recorded during the purge phase subsequent to first pulse and the corresponding fit, respectively. We have previously shown the lowering of the DoD (Fig. 1c) with an increase in the growth temperature. As a result, a less defective material induces an overall steeper slope during the exposure window (Fig. 4c). These findings are consistent with the conclusions achieved in our previous work [39]. In that paper, MLG synthesized *via* different routes, *i.e.* liquid phase exfoliation, mechanical cleavage and CVD, presented different types of defects associated to the synthesizing routes, whereas in this report, we study the correlation existing between the DoD intrinsically induced by the CVD-process and the kinetics of interaction with the analyte. In particular, since defects represent high-energy binding sites [20], the adsorption of molecules onto these sites results in a lower signal variation than that induced by low-energy binding sites, such as sp^2-bonded carbon [59–61]. The rate of response results in the different slope of the lines during the NO_2 pulse. Going into more details on either the nature of the defects or the interaction mechanism between the analyte molecules and the adsorption sites are out of the focus of the present report.

MLG850, that is the most defective material, shows the lowest current increase with a slope of $4.5 \cdot 10^{-5}$/min (black line). As the growth temperature increases while decreasing the DoD, it seems that the analyte's molecules are interacting less intensely with the sensing layer, resulting in a higher slope. The MLG935-based device (green line) reaches the maximum value of the slope ($24.6 \cdot 10^{-5}$/min), suggesting the lowest interaction with the bind-
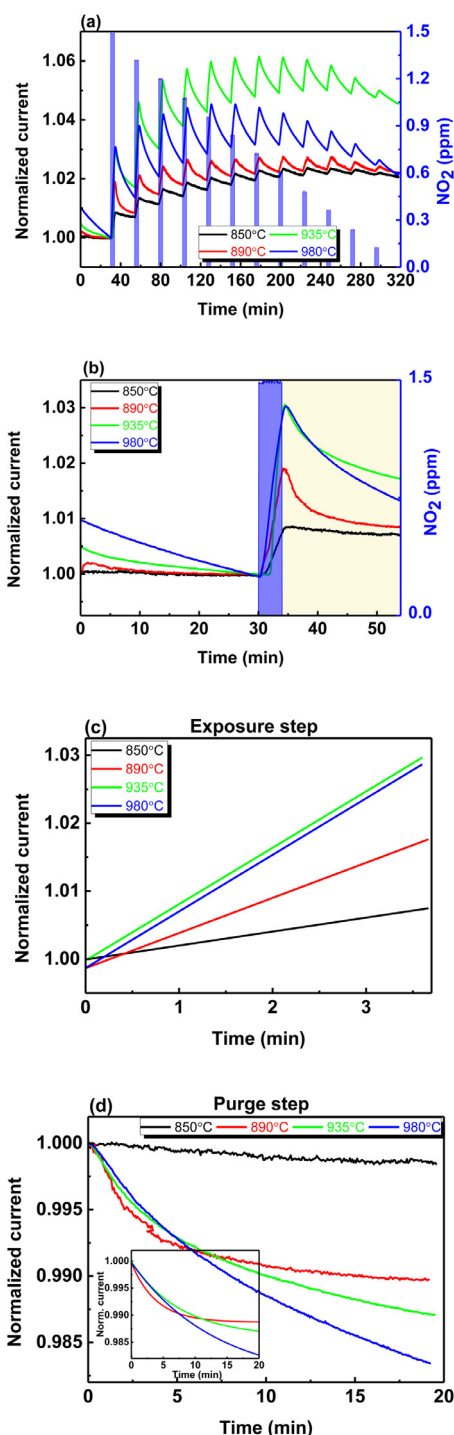
Fig. 5. (a) Real-time behavior of the current of the four sensors upon subsequent NO$_2$ exposures at different concentrations (blue rectangles). The graphs are normalized to the current value at the gas inlet of the first pulse. (b) Close-up of the first step from panel (a). (c) - (d) Fit of the graphs shown in panel (b) (blue rectangle) and magnification of the decreasing part of the signal recorded during the pulse at 1.5 ppm of NO$_2$ (yellow rectangle), respectively. The curves are normalized to the value of current at the inlet (c) and stop (d) of the gas flow in the test chamber. Inset: fit of the graphs in the panel (d). As the fit of the black curve (MLG850) does not converge, it is omitted from the Inset.

ing sites. Although the DoD is slightly reduced for MLG980 compared to MLG935 (see Fig. 1c), the plot of the MLG980-based device (blue line) shows a smaller gradient (14.1·10^{-5}/min) than that related to MLG935. It is very likely that around the growth temperature of 935 °C there might be a saturation of the trend previously

Table 3

Parameters related to the sensing properties of MLG as determined from Fig. 4c-d. R^2 shows the fit regression of the data of the purge phase.

Growth temperature (°C)	Slope (10^{-5}/min)	Relaxation time (s)	R^2
850	4.5	N/A	N/A
890	8.6	232	0.990
935	24.6	460	0.994
980	14.1	793	0.996

observed, preventing a further enhancement of the behavior of the other three samples.

Our hypothesis on the correlation between the DoD and the sensing properties is partly validated by analyzing the behavior of the transient during the purge step when only the buffer gas is introduced in the test chamber (Fig. 5d). Based on the growth temperature and, in turn, on the DoD, the devices tend to differently restore to the condition shown prior the exposure. While decreasing the DoD (increasing the growth temperature), the signal ranges from an almost absence of a change (MLG850, black line) to a moderately restored condition (MLG980, blue line) (Fig. 5d). The fits reported in the inset enable us to quantify this tendency. As no external energy, such as thermal heating or ultra-violet illumination, is supplied to the devices to promote the desorption from MLG, the current during the purge step can be treated as a spontaneous decay and fitted with a single exponential. Apart from the black curve showing no convergence (Fig. 5d), the values of R^2 (Table 3) show the close match between the experimental data and the fit (Fig. 5d inset). The relaxation time estimated from the three plots shows that the lower the DoD, the higher the constant of relaxation time constant and the faster the tendency to restore the conditions prior to the exposure (Table 3). This is a consequence of the DoD increasing, therefore the feed molecules become more strongly adsorbed and desorption is obstructed, especially when working at room temperature such as in our case [19,38,62]. We believe that the spontaneous desorption of the molecules enables the identification of the sensing properties of MLG, especially during the purge step. In that respect, here we ascribe the absence of any decreasing signal observed for the MLG850-based device to the strongest adsorption of the molecules with the most defective material.

Finally, Figure S6 reports the analysis described so far as performed on the second pulse of the series reported in Fig. 5a. We show that, independently from the injected NO$_2$ concentration of the pulse, the trend of both slope and relation time is well-aligned with the prior conclusions (Table S1). The outcomes thus highlight that the sensing properties, and eventually the sensitivity, of the carbon-based materials can be tuned already during the growth phase of the materials, without performing any post-growth treatment onto the sensing layer.

4. Conclusions

We synthesized MLG on pre-patterned Mo catalyst layer by CVD process varying the growth temperature. We showed that as the growth temperature increases, the defects spontaneously induced during the CVD process are reduced and a more organized structure of MLG is determined.

Through the resistors based on MLG, we analysed the influence of the defects on the sensing properties of MLG upon NO$_2$ exposure.

We highlighted that, while lowering the density of defects, the interaction with the analyte's molecules is overall less intense during the exposure windows. In turn, when the target gas is removed, the adsorbed molecules remain less attached to MLG, the relaxation time is higher and the restoration of the conditions prior

the exposure is favored. In conclusion, our findings show the feasibility of tuning the sensing properties of a material already operating during the synthesis process overcoming any post-growth process.

Declaration of Competing Interest

The authors declare that they have no known competing financial interests or personal relationships that could have appeared to influence the work reported in this paper.

Author contributions

F.R. conceived the idea of the work, fabricated the devices, performed the sensing measurements, analysed the data, wrote the original draft, reviewed and edited the manuscript. S.V. assisted with the fabrication of the devices and Raman measurements. R.S. performed the AFM measurements. O.H and C.J.B performed and assisted in the interpretation of XPS data. H.S. assisted in the interpretation of the Raman data and in the outline of the manuscript. P.M.S and G.S.D. supervised the manuscript. All authors have read and agreed to the published version of the manuscript.

Supplementary materials

Supplementary material associated with this article can be found, in the online version, at doi:10.1016/j.cartre.2021.100024.

References

[1] D.W. Boukhvalov, M.I. Katsnelson, Chemical functionalization of graphene with defects, Nano Lett 8 (2008) 4373–4379, doi:10.1088/0953-8984/21/34/344205.

[2] M.A. Pimenta, G. Dresselhaus, M.S. Dresselhaus, L.G. Cançado, A. Jorio, R. Saito, Studying disorder in graphite-based systems by Raman spectroscopy, Phys. Chem. Chem. Phys. 9 (2007) 1276–1291, doi:10.1039/b613962k.

[3] G.E. Collins, N.R. Armstrong, J.W. Pankow, C. Oden, R. Brina, C. Arbour, J.-P. Dodelet, Thin film sensors: the role of defects and impurity sites in controlling sensor response and selectivity, J. Vac. Sci. Technol. A Vacuum, Surfaces, Film. 11 (1993) 1383–1391, doi:10.1116/1.578558.

[4] D.W. Boukhvalov, M.I. Katsnelson, Chemical functionalization of graphene, J. Phys. Condens. Matter Chem. 21 (2009) 344205, doi:10.1021/nl802234n.

[5] O.V. Yazyev, S.G. Louie, Topological defects in graphene: dislocations and grain boundaries, Phys. Rev. B - Condens. Matter Mater. Phys. 81 (2010) 1–7, doi:10.1103/PhysRevB.81.195420.

[6] Y. Liu, H. Liu, Y. Chu, Y. Cui, T. Hayasaka, V. Dasaka, L. Nguyen, L. Lin, Defect-induced gas adsorption on graphene transistors, Adv. Mater. Interfaces. 5 (2018) 1–8, doi:10.1002/admi.201701640.

[7] T.O. Wehling, K.S. Novoselov, S.V. Morozov, E.E. Vdovin, M.I. Katsnelson, A.K. Geim, A.I. Lichtenstein, Molecular doping of graphene, Nano Lett 8 (2008) 173–177, doi:10.1021/nl072364w.

[8] S. Varghese, S. Varghese, S. Swaminathan, K. Singh, V. Mittal, Two-dimensional materials for sensing: graphene and beyond, Electronics (Basel) 4 (2015) 651–687, doi:10.3390/electronics4030651.

[9] S.S. Varghese, S. Lonkar, K.K. Singh, S. Swaminathan, A. Abdala, Recent advances in graphene based gas sensors, Sensors Actuators, B Chem 218 (2015) 160–183, doi:10.1016/j.snb.2015.04.062.

[10] Y.H. Zhang, Y. Bin Chen, K.G. Zhou, C.H. Liu, J. Zeng, H.L. Zhang, Y. Peng, Improving gas sensing properties of graphene by introducing dopants and defects: a first-principles study, Nanotechnology 20 (2009) 185504, doi:10.1088/0957-4484/20/18/185504.

[11] C. Ma, X. Shao, D. Cao, Nitrogen-doped graphene as an excellent candidate for selective gas sensing, Sci. China Chem. 57 (2014) 911–917, doi:10.1007/s11426-014-5066-2.

[12] A. Salehi-Khojin, D. Estrada, K.Y. Lin, M.H. Bae, F. Xiong, E. Pop, R.I. Masel, Polycrystalline graphene ribbons as chemiresistors, Adv. Mater. 24 (2012) 53–57, doi:10.1002/adma.201102663.

[13] A. Cagliani, D.M.A. Mackenzie, L.K. Tschammer, F. Pizzocchero, K. Almdal, P. Bøggild, Large-area nanopatterned graphene for ultrasensitive gas sensing, Nano Res 7 (2014) 743–754, doi:10.1007/s12274-014-0435-x.

[14] Y. Hajati, T. Blom, S.H.M. Jafri, S. Haldar, S. Bhandary, M.Z. Shoushtari, O. Eriksson, B. Sanyal, K. Leifer, Improved gas sensing activity in structurally defected bilayer graphene, Nanotechnology (2012) 23, doi:10.1088/0957-4484/23/50/505501.

[15] O.Y. Fangping, B. Huang, Z. Li, J. Xiao, H. Wang, H. Xu, Chemical functionalization of graphene nanoribbons by carboxyl groups on stone-wales defects, J. Phys. Chem. C. 112 (2008) 12003–12007, doi:10.1021/jp710547x.

[16] L.H. Zhang, Y. Shi, Y. Wang, N.R. Shiju, Nanocarbon catalysts: recent understanding regarding the active sites, Adv. Sci. 7 (2020), doi:10.1002/advs.201902126.

[17] G. Ruiz-Soria, A. Pérez Paz, M. Sauer, D.J. Mowbray, P. Lacovig, M. Dalmiglio, S. Lizzit, K. Yanagi, A. Rubio, A. Goldoni, P. Ayala, T. Pichler, Revealing the adsorption mechanisms of nitroxides on ultrapure, metallicity-sorted carbon nanotubes, ACS Nano 8 (2014) 1375–1383, doi:10.1021/nn405114z.

[18] M. Gautam, A.H. Jayatissa, Adsorption kinetics of ammonia sensing by graphene films decorated with platinum nanoparticles, J. Appl. Phys. 111 (2012), doi:10.1063/1.4714552.

[19] M.G. Chung, D.H. Kim, H.M. Lee, T. Kim, J.H. Choi, D.K. Seo, J.B. Yoo, S.H. Hong, T.J. Kang, Y.H. Kim, Highly sensitive NO 2 gas sensor based on ozone treated graphene, Sens. Actuators, B Chem. 166–167 (2012) 172–176, doi:10.1016/j.snb.2012.02.036.

[20] F. Banhart, J. Kotakoski, A.V. Krasheninnikov, Structural defects in graphene, ACS Nano 5 (2011) 26–41, doi:10.1021/nn102598m.

[21] G. Lee, G. Yang, A. Cho, J.W. Han, J. Kim, Defect-engineered graphene chemical sensors with ultrahigh sensitivity, Phys. Chem. Chem. Phys. 18 (2016) 14198–14204, doi:10.1039/C5CP04422G.

[22] G.C. Mastrapa, F.L. Freire, Plasma-treated CVD graphene gas sensor performance in environmental condition: the role of defects on sensitivity, J. Sensors. (2019) 2019, doi:10.1155/2019/5492583.

[23] F. Ricciardella, S. Vollebregt, T. Polichetti, M. Miscuglio, B. Alfano, M.L. Miglietta, E. Massera, G. Di Francia, P.M. Sarro, Effects of graphene defects on gas sensing properties towards NO 2 detection, Nanoscale 9 (2017) 6085–6093, doi:10.1039/C7NR01120B.

[24] A. Isacsson, A.W. Cummings, L. Colombo, L. Colombo, J.M. Kinaret, S. Roche, Scaling properties of polycrystalline graphene: a review, 2D Mater 4 (2017), doi:10.1088/2053-1583/aa5147.

[25] C. Tan, X. Cao, X.J. Wu, Q. He, J. Yang, X. Zhang, J. Chen, W. Zhao, S. Han, G.H. Nam, M. Sindoro, H. Zhang, Recent advances in ultrathin two-dimensional nanomaterials, Chem. Rev 117 (2017) 6225–6331, doi:10.1021/acs.chemrev.6b00558.

[26] B. Deng, Z. Liu, H. Peng, Toward mass production of CVD graphene films, Adv. Mater. 31 (2019) 1–25, doi:10.1002/adma.201800996.

[27] W. Tian, W. Li, W. Yu, X. Liu, A review on lattice defects in graphene: types generation effects and regulation, Micromachines (Basel) 8 (2017), doi:10.3390/mi8050163.

[28] E.J. Duplock, M. Scheffler, P.J.D. Lindan, Hallmark of perfect graphene, Phys. Rev. Lett. 92 (2004) 1–4, doi:10.1103/PhysRevLett.92.225502.

[29] O. Cretu, A.V. Krasheninnikov, J.A. Rodríguez-Manzo, L. Sun, R.M. Nieminen, F. Banhart, Migration and localization of metal atoms on strained graphene, Phys. Rev. Lett. 105 (2010) 1–4, doi:10.1103/PhysRevLett.105.196102.

[30] H. Terrones, R. Lv, M. Terrones, M.S. Dresselhaus, The role of defects and doping in 2D graphene sheets and 1D nanoribbons, Reports Prog. Phys. 75 (2012) 062501, doi:10.1088/0034-4885/75/6/062501.

[31] Z. Lin, B.R. Carvalho, E. Kahn, R. Lv, R. Rao, H. Terrones, M.A. Pimenta, M. Terrones, Defect engineering of two-dimensional transition metal dichalcogenides, 2D Mater 3 (2016) 022002, doi:10.1088/2053-1583/3/2/022002.

[32] Y.Z. Hong, W.H. Chiang, H.C. Tsai, M.C. Chuang, Y.C. Kuo, L.Y. Chang, C.H. Chen, J.D. White, W.Y. Woon, Local oxidation and reduction of graphene, Nanotechnology 28 (2017), doi:10.1088/1361-6528/aa802d.

[33] B. Vasić, U. Ralević, K. Cvetanović, M. Smiljanić, R. Gajić, M. Spasenović, S. Vollebregt, Low-friction, wear-resistant, and electrically homogeneous multilayer graphene grown by chemical vapor deposition on molybdenum, Appl. Surf. Sci. 509 (2020) 144792, doi:10.1016/j.apsusc.2019.144792.

[34] F. Ricciardella, S. Vollebregt, T. Polichetti, B. Alfano, E. Massera, P.M. Sarro, High sensitive gas sensors realized by a transfer-free process of CVD graphene, in: Proc. IEEE Sensors, 2016, pp. 697–699, doi:10.1109/ICSENS.2016.7808638. n.d.:.

[35] F. Ricciardella, S. Vollebregt, T. Polichetti, B. Alfano, E. Massera, P.M. Sarro, An innovative approach to overcome saturation and recovery issues of CVD graphene-based gas sensors, in: Proc. IEEE Sensors, 2017, pp. 1224–1226, doi:10.1109/ICSENS.2017.8234284. n.d.:.

[36] O. Leenaerts, B. Partoens, F.M. Peeters, Adsorption of H2 O, N H3, CO, N O2, and NO on graphene: a first-principles study, Phys. Rev. B - Condens. Matter Mater. Phys. 77 (2008) 1–6, doi:10.1103/PhysRevB.77.125416.

[37] F. Ricciardella, S. Vollebregt, T. Polichetti, P.M. Sarro, Low-humidity sensing properties of multi-layered graphene grown by chemical vapor deposition, Sensors 20 (2020) 3174–3184, doi:10.3390/s20113174.

[38] F. Ricciardella, T. Polichetti, S. Vollebregt, B. Alfano, E. Massera, L. Sarro, Analysis of a calibration method for non-stationary CVD multi-layered graphene-based gas sensors, Nanotechnology 30 (2019) 385501, doi:10.1088/1361-6528/ab2aac.

[39] F. Ricciardella, S. Vollebregt, T. Polichetti, M. Miscuglio, B. Alfano, M.L. Miglietta, E. Massera, G. Di Francia, P.M. Sarro, Effects of graphene defects on gas sensing properties towards NO2 detection, Nanoscale 9 (2017) 6085–6093, doi:10.1039/c7nr01120b.

[40] F. Ricciardella, S. Vollebregt, T. Polichetti, B. Alfano, E. Massera, P.M. Sarro, Low temperature CVD grown graphene for highly selective gas sensors working under ambient conditions, Proceedings 1 (2017) 445–448, doi:10.3390/proceedings1040445.

[41] S. Vollebregt, B. Alfano, F. Ricciardella, A.J.M. Giesbers, Y. Grachova, H.W. Van Zeijl, T. Polichetti, P.M. Sarro, A transfer-free wafer-scale CVD graphene fabrication process for MEMS/NEMS sensors, in: Proc. IEEE Int. Conf. Micro Electro Mech. Syst., 2016, doi:10.1109/MEMSYS.2016.7421546.

[42] A. Eckmann, A. Felten, A. Mishchenko, L. Britnell, R. Krupke, K.S. Novoselov, C. Casiraghi, Probing the nature of defects in graphene by Raman spectroscopy, Nano Lett 12 (2012) 3925–3930, doi:10.1021/nl300901a.

[43] L.M. Malard, M.A. Pimenta, G. Dresselhaus, M.S. Dresselhaus, Raman spectroscopy in graphene, Phys. Rep. 473 (2009) 51–87, doi:10.1016/j.physrep.2009.02.003.

[44] A. Eckmann, A. Felten, I. Verzhbitskiy, R. Davey, C. Casiraghi, Raman study on defective graphene: effect of the excitation energy, type, and amount of defects, Phys. Rev. B - Condens. Matter Mater. Phys. 88 (2013) 1–11, doi:10.1103/PhysRevB.88.035426.

[45] M.S. Dresselhaus, A. Jorio, A.G. Souza Filho, R. Saito, Defect characterization in graphene and carbon nanotubes using Raman spectroscopy, Philos. Trans. R. Soc. A Math. Phys. Eng. Sci. 368 (2010) 5355–5377, doi:10.1098/rsta.2010.0213.

[46] I. Pócsik, M. Hundhausen, M. Koós, L. Ley, Origin of the D peak in the Raman spectrum of microcrystalline graphite, J. Non. Cryst. Solids. 227–230 (1998) 1083–1086, doi:10.1016/S0022-3093(98)00349-4.

[47] M.J. Matthews, M.A. Pimenta, Origin of dispersive effects of the Raman D band in carbon materials, Phys. Rev. B. 59 (1999) 6585–6588, doi:10.1103/PhysRevB.59.R6585.

[48] M. Regmi, M.F. Chisholm, G. Eres, The effect of growth parameters on the intrinsic properties of large-area single layer graphene grown by chemical vapor deposition on Cu, Carbon N Y 50 (2012) 134–141, doi:10.1016/j.carbon.2011.07.063.

[49] C.M. Seah, S.P. Chai, A.R. Mohamed, Mechanisms of graphene growth by chemical vapour deposition on transition metals, Carbon N Y 70 (2014) 1–21, doi:10.1016/j.carbon.2013.12.073.

[50] G.-H.J. Byeong-Joo Lee, Comparative study on graphene growth mechanism using Ni films, Ni/Mo sheets, and Pt substrates, Appl. Phys. A. 116 (2014) 15–24.

[51] H.C. Lee, W.W. Liu, S.P. Chai, A.R. Mohamed, A. Aziz, C.S. Khe, N.M.S. Hidayah, U. Hashim, Review of the synthesis, transfer, characterization and growth mechanisms of single and multilayer graphene, RSC Adv 7 (2017) 15644–15693, doi:10.1039/C7RA00392G.

[52] Y. Wu, G. Yu, H. Wang, B. Wang, Z. Chen, Y. Zhang, B. Weng, X. Shi, X. Xie, Z. Jin, X. Liu, Synthesis of large-area graphene on molybdenum foils by chemical vapor deposition, Carbon N Y 50 (2012) 5226–5231, doi:10.1016/j.carbon.2012.07.007.

[53] A. Reina, X. Jia, J. N.D. Ho, H. Son, V. Bulovic, M.S. Dresselhaus, J. Kong, Large area, few-layer graphene films on arbitrary substrates by chemical vapor deposition, Nano Lett 9 (2009) 30–35.

[54] F. Ricciardella, S. Vollebregt, B. Boshuizen, F.J.K. Danzl, I. Cesar, P. Spinelli, P.M. Sarro, Wafer-scale transfer-free process of multi-layered graphene grown by chemical vapor deposition, Mater. Res. Express. 7 (2020), doi:10.1088/2053-1591/ab771e.

[55] F. Ricciardella, S. Vollebregt, E. Kurganova, A.J.M. Giesbers, M. Ahmadi, L. Sarro, Growth of multi-layered graphene on molybdenum catalyst by solid phase reaction with amorphous carbon, 2D Mater 6 (2019) 035012, doi:10.1088/2053-1583/ab1518.

[56] P. Lespade, A. Marchand, M. Couzi, F. Cruege, Characterization of carbon-carbon composites by Raman microprobe, Carbon N Y 22 (1984) 375–385.

[57] J. Romijn, S. Vollebregt, R.J. Dolleman, M. Singh, H.S.J. Van Der Zant, P.G. Steeneken, P.M. Sarro, A miniaturized low power pirani pressure sensor based on suspended graphene, in: Proc. NEMS 2018 - 13th Annu. IEEE Int. Conf. Nano/Micro Eng. Mol. Syst., 2018, pp. 11–14, doi:10.1109/NEMS.2018.8556902.

[58] G. Lu, S. Park, K. Yu, R.S. Ruoff, L.E. Ocola, D. Rosenmann, J. Chen, L.U.E.T. Al, Toward practical gas sensing with highly reduced graphene oxide : device-to-device variations, ACS Nano 5 (2011) 1154–1164, doi:10.1021/Nn102803q.

[59] J.T. Robinson, F.K. Perkins, E.S. Snow, Z. Wei, P.E. Sheehan, Reduced graphene oxide molecular sensors, Nano Lett. 8 (2008) 3137–3140, doi:10.1021/nl8013007.

[60] H. Choi, H.Y. Jeong, D.-S. Lee, C.-G. Choi, S.-.Y. Choi, Flexible NO 2 gas sensor using multilayer graphene films by chemical vapor deposition, Carbon Lett. 14 (2013) 186–189, doi:10.5714/CL.2013.14.3.186.

[61] H. Li, Z. Yin, Q. He, H. Li, X. Huang, G. Lu, D.W.H. Fam, A.I.Y. Tok, Q. Zhang, H. Zhang, Fabrication of single- and multilayer MoS 2 film-based field-effect transistors for sensing NO at room temperature, Small 8 (2012) 63–67, doi:10.1002/smll.201101016.

[62] G. Ko, H.-.Y. Kim, J. Ahn, Y.-.M. Park, K.-.Y. Lee, J. Kim, Graphene-based nitrogen dioxide gas sensors, Curr. Appl. Phys. 10 (2010) 1002–1004, doi:10.1016/J.CAP.2009.12.024.